MISSOURI S&T

Missouri University of Science and Technology

Scholars' Mine

International Specialty Conference on Cold-Formed Steel Structures

Wei-Wen Yu International Specialty Conference on Cold-Formed Steel Structures 2016

Nov 10th, 12:00 AM - 12:00 AM

A Combined Direct Analysis and Direct Strength Approach to Predict the Flexural Strength of Z-Purlins with Paired Torsion Braces

Michael W. Seek

Chris Ramseyer

Ian Kaplan

Follow this and additional works at: https://scholarsmine.mst.edu/isccss

Part of the Structural Engineering Commons

Recommended Citation
Seek, Michael W.; Ramseyer, Chris; and Kaplan, Ian, "A Combined Direct Analysis and Direct Strength Approach to Predict the Flexural Strength of Z-Purlins with Paired Torsion Braces" (2016). *International Specialty Conference on Cold-Formed Steel Structures*. 5.
https://scholarsmine.mst.edu/isccss/23iccfss/session9/5

A Combined Direct Analysis and Direct Strength Approach to Predict the Flexural Strength of Z-Purlins with Paired Torsion Braces

Michael W. Seek[1], Chris Ramseyer[2] and Ian Kaplan[3]

Abstract

A series of 12 Base Tests for Z-section purlins with paired interior torsional braces and one flange attached to a flexible horizontal diaphragm are evaluated with the Direct Strength Method. Rather than use the conventional constrained bending stress approximation, a direct analysis philosophy is adopted where cross section stress distributions are calculated using a displacement compatibility approach. With a flexible diaphragm typical of a standing seam roof system, these stresses can deviate substantially from the constrained bending approximation and can significantly impact predicted local and distortional buckling behavior. The displacement compatibility approach incorporates estimates of load imbalances and second order effects that result from the standard base test procedure. Predicted local and distortional buckling strength shows good correlation to tested strength.

Introduction

Z-section purlins with third point torsion braces have gained popularity in recent years because of their efficiency and relatively high reduction factors (R-factors). The third point torsion braces eliminate the need to provide external lateral anchors along the span. As purlins deflect laterally, the torsion braces absorb second order torsions and allow for larger lateral deflections without significant strength degradation. Applying the conventional global lateral torsional buckling, local buckling, and distortional bucking equations presented in the AISI Specification (AISI 2012), typically results in very conservative predictions of purlin capacity. It is typically assumed when applying these methods, that a the stress distribution in the purlin cross section matches that of constrained bending which requires that the purlin is constrained to deform only

[1] Assistant Professor, Old Dominion University, Norfolk, VA
[2] Associate Professor, University of Oklahoma, Norman, OK
[3] Graduate Student, Old Dominion University, Norfolk, VA

in the plane of the web. In reality, the actual stress distribution falls somewhere between the constrained bending and the unsymmetric bending cases depending primarily on the flexibility of the diaphragm

The Component Stiffness Method is a displacement compatibility method to predict brace forces in purlin systems. A procedure for analyzing purlin systems with third point torsional braces is presented in the AISI Design Guide for Cold Formed Steel Purlin Roof Framing Systems (AISI, 2009) and is refined by Seek (2014). The procedure not only calculates the brace forces but provides insight into the forces of the components of the system as well as the deformations of the system. With the component forces and system deformations, the stresses in the purlin cross section can be determined from conventional mechanics.

Elastic stresses calculated by incorporating the flexibility of the purlin system deviate substantially from those approximated by constrained bending. Peak compressive stresses shift from the flange stiffener to the junction between the web and flange, impacting both the local and distortional bucking behavior. The shift in stresses decreases the likelihood of flange or stiffener buckling and increases the likelihood of local buckling at the web-flange juncture. The distortional buckling strength is increased or may even be eliminated as a buckling mode as compressive stresses at the tip of the flange are reduced.

This paper presents a procedure to calculate the actual distribution of stresses throughout the cross section of a Z-section from the applied pressures of a Base Test (AISI S908, 2013). The procedure includes methods to approximate the additional stresses introduced by load imbalances resulting from the standard Base Test procedure, by concentrated forces at the torsional brace locations, and geometric second order effects caused by the diaphragm deformation. From the calculated stress distribution, the local and distortional buckling strength can be calculated using the Direct Strength method. The methodology is compared to a series of twelve base tests: 3 tests each of 8Z16, 8Z12, 10Z16 and 10Z12 cross sections. In all cases, the predicted strength shows good correlation with the Base Test results.

Calculation of Cross Section Stresses
The Base Test is performed in a vacuum chamber on a full scale simple span specimen representing a roof system. The specimen is constructed with two purlins spaced at 5'-0" typically with panels attached to the top flange of the purlin. To engage the resistance of the diaphragm, both purlins are oriented with their flanges facing in the same direction, referred to the "uphill" direction or ridge side. The panels, typically 7'-0" long, overhang the purlins by 1'-0" on each side. The specimen is covered with plastic sheathing that is sealed along

the edges of the vacuum chamber. Differential pressures are exerted on the specimen by evacuating the chamber.

The Base Test Method produces a consistent and uniform pressure along the panels attached to the top of the purlin via clips. However, there are slight imbalances inherent in the test setup. These imbalances typically shift greater load to the purlin on the "downhill" side causing the downhill, or "eave" purlin to fail first. This phenomenon has long been recognized and the Base Test standard provides guidance on quantifying the load imbalance when the downhill purlin is the first to fail. When paired torsional braces are used, the torsional braces contribute to the load imbalance and therefore a slightly different approach than that presented in the Base Test standard must be used. For large lateral deformations, the imbalance of forces may shift to increase the downward force on the ridge purlin. This less understood phenomenon can be quantified by the presented method as well.
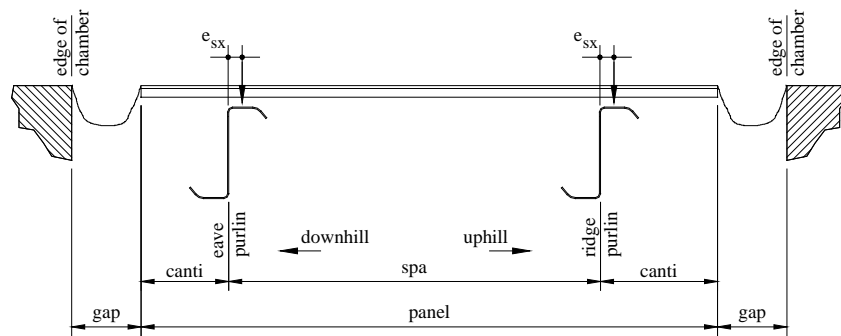
**Figure 1. Base Test Layout and Nomenclature**

The layout of the specimen used in the base test and the nomenclature used in the calculation of the uniform forces on the purlin is shown in Figure 1. The dead load of the specimen including the weight of the panel, purlin and insulation is u_d and the applied pressure is u_p. To account for the differences between the eave and ridge purlin, the variable ξ is applied where $\xi = 1$ for the eave purlin and $\xi = -1$ for the ridge purlin. The balanced first order uniform force on each purlin is

$$w_{1st} = \frac{u_d \left(panel\right) + u_p \left(panel + gap\right)}{2} \tag{1}$$

To account for the eccentricity of the applied force at the panel as it is transferred to the purlin at an eccentricity e_{sx}, an additional uniform load, w_e is applied

$$w_e = w_{1st}\left(\frac{2e_{sx}}{spa}\right)\xi \tag{2}$$

The eccentricity of the load applied to the top flange is generally accepted as 1/3 of the flange width. The positive directions for load and displacement are shown in Figure 2.
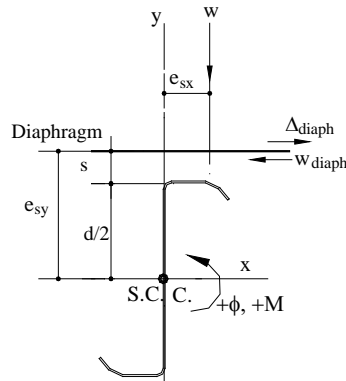
Figure 2. Nomenclature and Positive Load and Displacement Directions

As the pressure in the chamber is increased, the purlins will deflect laterally in the uphill direction. With this shift towards the ridge, the gap between the edge of the panel and the edge of the chamber opens at the eave and decreases at the ridge. As a result of this effect, the load is increased on the eave and correspondingly decreased at the ridge. This load has a parabolic distribution with the peak quantified as

$$w_{2nd} = u_p\left(\frac{\Delta_{diaph}}{2}\right)\left(\frac{panel}{spa}\right)\xi \tag{3}$$

The displacement of the diaphragm, Δ_{diaph} is calculated in Eq. 7 by enforcing displacement compatibility between the lateral deflection of the purlin and the resistance of the diaphragm. The total load contributing to the lateral displacement of the diaphragm after the dead loads are in place is

$$w_{panel} = u_d\left(panel + gap\right) \tag{4}$$

In Seek (2014), a method is presented to calculate the force introduced in the diaphragm for a system with third point torsional braces. The method can be further simplified if the purlin end restraints are considered to be rigid. For comparison to the base test, displacement compatibility is determined at the mid-span. The in plane force in the diaphragm is

$$w_{diaph} = \sigma \cdot w_{panel} \tag{5}$$

where

$$\sigma = \frac{\dfrac{5 \left(\dfrac{I_{xy}}{I_x} \right) L^4}{384 EI_{my}}}{\dfrac{5L^4}{384 EI_{my}} + \dfrac{L^2}{8G'(panel)}} \tag{6}$$

In the Eq. 6, I_{my} is the modified moment of inertia about the orthogonal y-axis as defined in Zetlin and Winter (1955). From the in plane force in the diaphragm, the lateral displacement of the diaphragm at mid-span is

$$\Delta_{diaph} = \frac{\sigma \cdot w_{panel} L^2}{8G'(panel)} \tag{7}$$

Torsion

The purlins in the base test are subjected to torsion both from the eccentricity of the applied load and the lateral resistance of the panel attached at the top flange. The torsion along the length of the purlin is balanced by the concentrated torques at the brace location. The uniform torque along the length of the purlin from first order effects is

$$t_{1st} = (w_{1st} + w_e \xi)(\sigma \cdot e_{sy} - e_{sx}) \tag{8}$$

The purlin is subject to additional second order torsions as a result of the lateral deformation of the system. Torsion results from both the load shift to the eave as the system displaces and the torsion induces as the mid-span of the purlin deflects laterally relative to the supports. Both of these torsions are approximated with a parabolic distribution with a peak torque per unit length equal to

$$t_{2nd} = -w_{2nd} \cdot e_{sx} \xi - (w_{1st} + (w_e + w_{2nd}) \xi) \Delta_{diaph} \tag{9}$$

The torsion along the length of the member is balanced by the paired torsion braces. The braces are assumed to be rigid and the magnitude of the torque is determined by enforcing displacement compatibility at the brace location. Pure

torsion effects can be ignored greatly simplify the calculations. The brace torque from first order load effects is

$$T_{1st} = -\frac{11}{30} t_{1st} L \tag{10}$$

The brace torque from the second order effects with a parabolic load distribution is

$$T_{2nd} = -\frac{602}{2025} t_{2nd} L \tag{11}$$

To balance the moments at each end of the torsion brace, there is vertical reaction, V, at each end of the brace in opposing directions as shown in Figure 3. The positive direction for the reaction on the purlin is in the gravity direction.
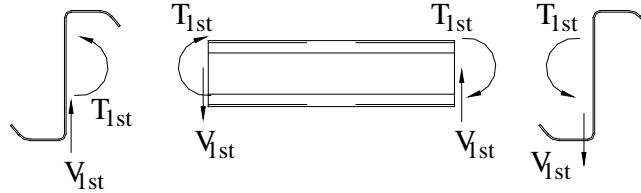
Figure 3. Balance of Forces for Torsional Brace

When the diaphragm is stiff, this balance of forces increases the load in the gravity direction on the eave purlin. For more flexible diaphragms, as second order effects increase, the balancing torques can be reversed, resulting in additional force in the gravity direction on the ridge purlin. The respective first order and second order brace reactions at each third point are

$$V_{1st} = \frac{2\left(\frac{11}{30}\right) w_{1st} L \left(\sigma \times e_{sy} - e_{sx}\right) \xi}{spa} \tag{12}$$

$$V_{2nd} = \frac{2\left(\frac{602}{2025}\right) w_{1st} \Delta_{diaph} L \xi}{spa} \tag{13}$$

Mid-span Bending and Warping Normal Stresses

The total mid-span moment about the orthogonal x-axis from combined first order and second order bending stresses is

$$M_{mid} = \left(w_{1st} + w_e\right)\frac{L^2}{8} + w_{2nd}\frac{5L^2}{48} + \left(V_{1st} + V_{2nd}\right)\frac{L}{3} \tag{14}$$

The bending normal stresses from biaxial bending of the cross section are calculated at each point along the cross section defined by coordinates (x,y) by

$$f_b = M_{mid} \left[\frac{-y}{I_{mx}} + \frac{x \dfrac{I_{xy}}{I_x}}{I_{my}} - \frac{x \cdot \sigma}{I_{my}} + \frac{y \dfrac{I_{xy}}{I_y} \sigma}{I_{mx}} \right] \quad (15)$$

The terms I_{mx} and I_{my} are the modified moments of inertia about the orthogonal x- and y- axes respectively. The normal stresses caused by warping torsion, f_w, are calculated

$$f_w = E \cdot W_N \cdot \phi'' \quad (16)$$

where W_N is the normalized warping function at a specific point on the cross section and $\phi``$ is the second derivative of the rotation function with respect to z due to the applied load. Guidance on calculating the normalized warping function for thin walled cross sections is provided in Cold-Formed Steel Design (Yu, 2010). The normalized warping function is calculated at the same coordinates (x,y) across the cross section as the bending normal stresses.

There are 3 rotation functions that need to be considered: 1) uniform torsion along span, 2) parabolic distribution along span, 3) concentrated torque at brace locations (3rd points). At the mid-span location, the rotation functions are:

Uniform Torsion

$$\phi_u'' = \frac{t_{1st}}{GJ} \left(\frac{1}{\cosh\left(\dfrac{L}{2a}\right)} - 1 \right) \quad (17)$$

Parabolic Torsion Distribution

$$\phi_p'' = \frac{t_{2nd}}{GJ} \left[\frac{8a^2}{L^2} \left(1 - \frac{1}{\cosh\left(\dfrac{L}{2a}\right)} \right) - 1 \right] \quad (18)$$

Concentrated Torsion at Brace Location (3rd Points)

$$\phi_{3rd}" = \frac{T_{1st} + T_{2nd}}{GJ}\left(\frac{1}{a}\right)\left[\sinh\left(\frac{L}{2a}\right)\left(\frac{\sinh\left(\frac{L}{3a}\right)+\sinh\left(\frac{2L}{3a}\right)}{\tanh\left(\frac{L}{a}\right)}-\cosh\left(\frac{2L}{3a}\right)\right)-\cosh\left(\frac{L}{2a}\right)\sinh\left(\frac{L}{3a}\right)\right]$$

(19)

Combining equations 17, 18 and 19 into equation 16, the normal stress resulting from warping torsion at each coordinate on the cross section is calculated

$$f_w = E \cdot W_N \cdot \left(\phi_u " + \phi_p " + \phi_{3rd}"\right)$$

(20)

The net normal stresses are the combined sum of the bending stresses and warping stresses.

Comparison to Base Test Results

Traditionally, Base Test results are used to predict the strength of a purlin in a roof system by applying a reduction factor (R-factor) to the nominal local buckling strength of the purlin cross section. The local buckling strength is determined using a constrained bending stress distribution. With a flexible diaphragm, the stresses deviate substantially from the constrained bending assumption. Peak compressive stresses occur at the intersection of the web and flange and are significantly reduced at the tip of the compressive flange.

In this study, the calculation of stresses in the cross section includes the effects of lateral deformation and torsion. With the more realistic distribution of stresses, local and distortional buckling strengths are calculated using the Direct Strength method. When compared to base test results, there is good correlation between predicted moment strength and the test results.

The base tests investigated were performed at the University of Oklahoma and reported by Emde (2010). Four purlin cross sections were investigated: 8Z16, 8Z12, 10Z16, and 10Z12, where the first number represents the nominal depth and the second number represents the material gauge. Although more than three tests were performed for each purlin series with varying bracing configurations, only the three tests for each cross section used to determine the R-factors are investigated in this study.

The purlins with an 8 inch nominal depth were tested on a span of 27'-0". The torsional braces were located at 10'-6" from each end of the purlin leaving a 6'-0" space between the braces in the middle. The purlins with a 10" nominal depth were tested on a 30'-0" span with torsional braces located at 11'-6" from each end of the span leaving a 7'-0" space between the braces in the middle. It should be noted that the analysis provided in this paper is based on braces

located at the third points along the span. It is believed that the resulting difference in stresses is minimal as a result of this discrepancy.

Purlin section properties are calculated based on the reported cross section measurements and the diaphragm stiffness, G', is estimated by comparing the calculated deflection to the measured deflection. Some adjustments to the diaphragm stiffness are required between test series to better align the measured and calculated deflections. The more heavily loaded diaphragms required a reduced diaphragm stiffness to align deflections. This is consistent with tests on diaphragms where a softening effect is typically experienced as shear in the diaphragm is increased. The estimated diaphragm stiffness and the measured and calculated deflections are shown in Table 1.

Table 1. Comparison of Tested to Calculated Diaphragm Deflection

Test	Applied Pressure (psf)	Estimated G' (lb/in)	Δ_{diaph} Calculated (in)	Δ_{diaph} Measured (in)	Deflection Ratio
8Z16-1A	17.68	230	1.78	1.86	L/174
8Z16-1D	19.07	230	1.93	1.85	L/175
8Z16-1G	16.54	230	1.65	1.33	L/244
8Z12-2D	37.65	110	5.97	6.17	L/53
8Z12-2E	27.15	110	4.27	5.29	L/61
8Z12-2F	37.87	110	5.93	5.94	L/55
10Z16-3A	19.46	300	1.74	1.18	L/305
10Z16-3D	18.54	300	1.59	1.53	L/235
10Z16-3E	16.55	300	1.37	1.49	L/242
10Z12-4A	45.02	160	5.72	5.59	L/64
10Z12-4C	40.02	160	5.06	5.75	L/63
10Z12-5A	44.57	200	4.96	4.72	L/76

To facilitate the finite strip analysis of the section, the cross section is subdivided. Each element of the cross section (web, flange, stiffeners and radii) are divided into 4 equal segments resulting in 36 linear segments and 37 node points to describe the cross section.

Based on the reported dead load of the system and the pressure differential at failure, the stresses in the cross section at each node point is calculated. The moment supported by the purlin at this load level is calculated by Eq. 14 and is considered the test moment, M_{test}. In each test, the peak compressive stress, f_c occurs within the radius at the top flange-web juncture. To perform the finite strip analysis, the stresses in the cross section are scaled a factor of F_y/f_c. By

scaling the stresses, the peak compressive stress in the web-flange juncture is set to the yield stress (first yield point). The corresponding yield moment, M_y is calculated

$$M_y = M_{test}\frac{F_y}{f_c} \tag{21}$$

A finite strip analysis is performed using CUFSM v.4.05 (Li and Schafer, 2010) with the above scaled stresses to obtain the critical elastic local and distortional buckling moments, $M_{cr\ell}$ and M_{crd}, respectively. Although, the critical elastic distortional buckling moment can be affected by the rotational restraint provided by the connection to the sheathing, this contribution to strength is not considered in this analysis. The nominal local and distortional buckling strengths are calculated according to Section 1.2.2 of Appendix 1 of the AISI Specification (AISI, 2012). The controlling nominal moment strength is the minimum of the nominal local buckling strength and distortional buckling strength. The global flexural buckling strength was not considered in this analysis. The calculated nominal moment strength, M_n, was then compared to the maximum moment supported by the specimen in the test, M_{test}. The results of this analysis are presented in Table 2 for 8 inch nominal depth purlins and in Table 3 for 10 inch nominal depth purlins.

Table 2. Analysis Results for 8" Purlins

Section	8Z16			8Z12		
Test ID	1A	1D	1G	2D	2E	2F
Fy (ksi)	70.8	68.8	64.1	79.1	79.1	79.1
t (in)	.060	.060	.060	.103	.103	.103
u_d (psf)	2.62	2.65	2.66	3.18	3.18	3.2
u_p (psf)	17.68	19.07	16.54	37.65	27.15	37.87
f_c (ksi)	50.9	51.1	47.3	71.3	51.5	71.1
M_{test} (kip-ft)	7.074	7.153	6.684	14.113	10.469	14.193
F_y/f_c	1.416	1.421	1.373	1.110	1.530	1.113
Local load factor	0.56	0.62	0.63	1.39	1.44	1.4
Distortional Load Factor	0.73	0.68	0.78	1.86	1.86	1.86
$M_{n\ell}$ (kip-ft)	6.996	7.354	6.678	14.811	15.316	14.973
M_{nd} (kip-ft)	6.947	6.860	6.531	14.953	15.291	15.082
M_n (kip-ft)	6.947	6.860	6.531	14.811	15.291	14.973
M_{test}/M_n	1.02	1.04	1.02	0.95	0.68	0.95
Mean	1.03			0.86		
COV	0.01			0.15		

Table 3. Analysis Results for 10" Purlins

| Section	10Z16			10Z12		
Test ID	3A	3D	3E	4A	4C	5A
F_y (ksi)	56.1	68.3	63.9	67.1	65.8	65.4
t (in)	.064	.059	.059	.103	.104	.105
u_d (psf)	2.84	2.82	2.82	3.46	3.47	3.47
u_p (psf)	19.46	18.54	16.55	45.02	40.02	44.57
f_c (ksi)	50.9	51.1	47.3	71.3	51.5	71.1
M_{test} (kip-ft)	9.659	9.222	8.352	19.910	17.848	19.622
F_y/f_c	1.300	1.583	1.709	1.051	1.151	1.073
Local load factor	0.51	0.39	0.42	1.09	1.11	1.14
Distortional Load Factor	0.7	0.5	0.46	1.69	1.60	1.7
$M_{n\ell}$ (kip-ft)	8.490	8.985	9.017	18.300	18.066	18.686
M_{nd} (kip-ft)	8.569	8.716	8.235	19.427	18.751	19.583
M_n (kip-ft)	8.490	8.716	8.235	18.300	18.066	18.686
M_{test}/M_n	1.14	1.06	1.01	1.09	0.99	1.05
Mean	1.07			1.04		
COV	0.05			0.04		

Discussion of Results

For the constrained bending assumption to hold true for a purlin system with torsional braces, the diaphragm attached to the top flange of the purlin must be rigid. As diaphragm flexibility is introduced, the purlin is subjected to biaxial bending, causing a redistribution of stresses. In the top flange, compressive stresses are reduced at the flange tips and increased at the intersection between the flange and the web. The peak compressive stress occurs at this intersection between the web and flange. If a purlin is subjected to a uniform load parallel to its web, first yield will occur at the web-flange intersection at a much lower load level for a flexible diaphragm than with a rigid diaphragm. The more flexible the diaphragm, the less applied load required to reach first yield.

However, this change in stress distribution also changes the local and distortional buckling behavior. For local buckling, for a cross section with a constrained bending stress distribution, local buckling may occur in the web, flange or the flange stiffener. In the biaxial bending distribution, as stresses shift to the web-flange intersection, driving the controlling local buckling mode to web local buckling. Depending on the cross section, there may be little change in the local buckling load factor with this shift in stresses, however, the

first yield point will occur at lower load level. The shift in stresses to the web is supported by the test results, where the primary mode of failure observed was local buckling at the web-flange juncture.

For distortional buckling, when subjected to a constrained bending stress distribution, the flange stiffener loses effectiveness and the typically distortional mode is combined buckling of the flange and web. With a biaxial bending stress distribution, the stresses in the flange stiffener are reduced, maintaining its effectiveness in stabilizing the flange, and there is a stress gradient in the flange, reducing its tendency to buckle. If the biaxial bending is significant enough, the distortional buckling mode may be eliminated altogether.

A comparison between the finite strip results is shown for the flexible diaphragm case (10Z12-4C) and the constrained bending case (10Z12-4C-constrained) for the test 10Z12-4C in Figure 3. For local buckling, the biaxial bending case increases the stress gradient in the web, resulting in a slightly lower load factor than the constrained bending case. For distortional buckling, Figure 3 shows that the minima for the distortional buckling wavelength is eliminated for the biaxial bending case.
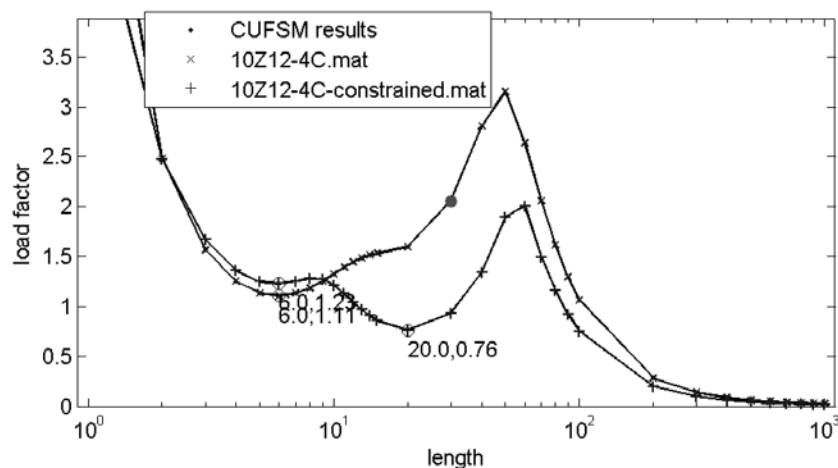
Figure 4. Comparison of Finite Strip Analysis Results

The 8Z16 series (8 in nominal depth, 16 gage material), showed excellent correlation between the predicted and tested strengths. The tests for the 8Z16 series showed the greatest consistency which explains the corresponding consistency of the predicted strength. Distortional buckling controlled the

strength of the cross section in all cases but was only slightly less than the local buckling strength. If the contribution of the panel to the distortional buckling strength was included, local buckling strength would likely control. In all cases, the predicted strength is slightly less than the tested strength and thus the predicted strength is conservative. Panel lateral deflections are consistent and close to the lateral deflection limit for systems with torsion braces (L/180).

The 8Z12 series experienced much larger deflections than the 8Z16 series as a result of the demands the higher supported loads place on the diaphragm. To match the calculated lateral deflections with the tested deflections, a more flexible diaphragm is modeled for the 8Z16 series tests. Diaphragms typically exhibit a softening as in-plane shear increases, so it is reasonable to use a lesser stiffness at higher loads. Because of the large lateral displacement and corresponding reduction of compressive stresses in the flange stiffener, distortional buckling strength is increased and local buckling is the primary failure mode. The predicted strength is higher than the tested strength. For tests 2D and 2F, this difference is slight (within 5%). However for test 2E, the difference is significant. Failure of this specimen may have been premature as a result of the test configuration. For series 8Z12, the difference between the predicted strength and tested strength may be the result of the assumption that the braces are rigid. As larger demands are placed on the braces, they will undergo larger deformation, affecting the extent to which the purlin is restrained. Unless these effects are accounted for, the predicted strength may exceed the tested strength.

The 10Z16 series, like the 8Z16 series, placed less demands on the diaphragm as a result of the lower applied loads. To match the predicted lateral deflections to the tested deflections, a stiffer diaphragm than the 8Z16 series is modeled. In all cases, the predicted strength is less than the tested strength. The distortional buckling strength and the local buckling strength are closely aligned but the distortional buckling strength generally controls. The 10Z16 series shows more variation (COV = 0.05) and the predicted strength is more conservative (7% on average) than the 8Z16 series. Nevertheless, the correlation between the predicted strength and tested strength is good.

For the 10Z12 series, the local buckling strength controlled. The finite strip analysis did not display a significant distortional buckling minima, but rather a slight plateau in the typical distortional buckling half-wavelength. A conservative load factor was chosen for distortional buckling but it did not reduce the predicted distortional buckling strength below the local buckling strength. The predicted strength is conservative but still very close to tested

strength (within 4% on average). The predicted strengths were consistent with a coefficient of variation of 0.04.

For the tests on the lighter gage material (8Z16 and 10Z16), the peak compressive stress at the web-flange juncture at the test failure pressure is significantly less than the yield stress. For the finite strip analysis, scale factors of approximately 1.4 were applied to the 8Z16 series and between 1.3 and 1.7 for the 10Z16 series. For the heavier 12 gage material, stress scale factors were on the order of 1.1 except for test 2E which may be an outlier. These scale factors correlate with the expectation that the thinner material will buckle at lower stress levels than the thicker material.

Conclusions

In the current design methodology for purlins with one flange attached to sheathing, there is a disconnect between the determination of flexural strength and the evaluation of the bracing. Flexural strength is determined based on the constrained bending assumption and bracing and anchorage forces are calculated with the understanding that the system is not perfectly constrained. This disconnect is further compounded by the fact that strength of a purlin system is determined by the base test in the horizontal position. With a flexible system, the deformations and corresponding stresses in the system on a sloped roof can be significantly different than on a flat roof.

The direct analysis methodology provided herein directly relates the extent to which a purlin is laterally restrained by the panel to the stresses in the cross section. The method shows the substantial deviation in stresses from the constrained bending assumption and that the first yield is realized at a lower applied load level than under constrained bending.

A direct analysis method is presented to evaluate the results of Base Tests on purlins with paired torsional braces. The method accounts for imbalances and some of the geometric second order effects inherent in the Base Test. By quantifying the lateral deformation of the diaphragm and the concentrated torque of the torsional braces, a realistic distribution of stresses across the cross section can be determined. With this distribution of stresses, a direct strength approach utilizing a finite strip analysis determines the nominal local and distortional buckling strengths.

The method was compared to a series of 12 base tests, subdivided into 3 tests each of 4 different purlin cross sections (8Z16, 8Z12, 10Z16, 10Z12). In all cases, the predicted flexural strength is closely aligned with the strength extrapolated from the test results. For all 12 tests, the mean ratio of M_{test} to M_n

is 1.0 with a coefficient of variation of 0.11. The correlation within each test series varies but in general the predicted strength is less than the tested strength.

This study is a preliminary work to explore the ability of the direct analysis method to predict the flexural capacity of purlins with torsional braces. Additional work is needed to develop equations for paired braces at any location along the span. Global buckling effects, stress distributions at locations other than the purlin mid-span, impacts of flexible braces and the effects of roof slope need to be explored. The correlation of the predicted results to the tested results are very promising. With additional refinements, the presented direct analysis method combined with the powerful direct strength method has the potential to greatly improve the ability to predict the flexural strength of purlins with paired torsional braces.

References

AISI (American Iron and Steel Institute). (2013) *S908-13 Base Test Method for Purlins Supporting a Standing Seam Roof System.* Washington, DC.

AISI (American Iron and Steel Institute). (2012). *North American Specification for the Design of Cold-Formed Steel Structural Members.* Washington, DC.

Emde, M. G. (2010) *Investigation of Torsional Bracing off Cold-Formed Steel Roofing Systems.* Master's Thesis. University of Oklahoma. Norman, OK.

Li, A., Schafer, B.W. (2010) "Buckling analysis of cold-formed steel members with general boundary conditions using CUFSM: conventional and constrained finite strip methods." Proceedings of the 20th International Specialty Conference on Cold-Formed Steel Structures.

Murray, T. M., Sears, J., and Seek, M. W. (2009). *D111-09 Design Guide for Cold-Formed Steel Purlin Roof Framing Systems.* American Iron and Steel Institute. Washington, DC.

Seek, M. W. (2014). "Improvements to the prediction of brace forces in Z-purlin roof systems with support + third point torsion bracing". Proceedings of the 22nd International Specialty Conference on Cold-Formed Steel Structures.

Yu, W. and R. A. Laboube. (2010) *Cold-Formed Steel Design, 4th ed.* John Wiley & Sons. Hoboken, NJ.

Zetlin, L and G. Winter (1955), "Unsymmetrical Bending of Beams with and without Lateral Bracing." *Journal of the Structural Division*, ASCE, Vol. 81, 1955.